Supplement of Atmos. Chem. Phys., 20, 8181–8200, 2020
https://doi.org/10.5194/acp-20-8181-2020-supplement

Atmospheric Chemistry and Physics
Open Access
EGU

Supplement of

Atmospheric reactivity and oxidation capacity during summer at a sub-urban site between Beijing and Tianjin

Yuan Yang et al.

Correspondence to: Yonghong Wang (yonghong.wang@helsinki.fi) and Yuesi Wang (wys@mail.iap.ac.cn)

Description of experimental method

O_3 was measured using a UV photometric O_3 analyzer (Model 49C/I, Thermo-Fisher Scientific, United States) with the detection limit of 2.0 ppb, precision of ±1.0 ppb, zero drift of less than 1.0 ppb $(24\ h)^{-1}$, span drift of less than 1% full scale per month, and response time of 10 s. NO_x was measured using a chemiluminescence NO_x Analyzer (Model 42C/I) with the detection limit of 0.4 ppb, precision of ±0.4 ppb, zero drift of less than 0.4 ppb $(24\ h)^{-1}$, span drift of less than 1% per 24 h, and response time of 40 s. NO_y was measured using a chemiluminescence NO-DIF-NOy Analyzer (Model 42C/I) with the detection limit of 50 ppt, span drift of less than 1% per 24 h, and response time of 60 s. SO_2 was measured using a pulsed fluorescence SO_2 analyzer (Model 43C/I) with the detection limit of 0.5 ppb, precision of 1% of reading or 1 ppb, zero drift of less than 1 ppb $(24\ h)^{-1}$, span drift of less than 0.5% full scale per 24 h, and response time of less than 20 s. CO was measured with a nondispersive infrared analyzer (Model 48I) with the detection limit of 0.4 ppm, a precision of 0.1 ppm, zero drift of less than 0.1 ppb $(24\ h)^{-1}$, span drift of less than 0.1% full scale per 24 h, and response time of less than 60 s. These measurement instruments were housed in a container that was equipped with an air conditioner. Ambient air samples were drawn through a 3-m PFA Teflon tube (outside diameter: 12.7 mm; inside diameter: 9.6 mm), and the sampling tube inlets were located 1m above the conditioner. High resolution (5 min averages) data sets of O_3, NO, NOx, NOy, SO_2 and CO were obtained, and hourly averaged data were used after applying strict data quality control. The sampling methods and instrument protocols as well as quality assurance/quality control (QA/QC) procedures for air quality monitoring are described in detail in the Chinese National Environmental Protection Standard, Automated Methods for Ambient Air Quality Monitoring (HJ/T 193–2005; State Environmental Protection Administration of China, 2006). The measurement techniques are the same as those used in (Wang et al., 2014;Xin et al., 2012).

Ambient NMVOCs were collected and analyzed continuously and automatically with a time resolution of 1 h using a custom-built gas chromatography-mass spectrometry/flame ionization detector (GC-MS/FID). The online GC-MS/FID system consisted of three major components: a cryogen-free cooling device for creating ultra-low temperatures (TH300, Wuhan Tianhong Environmental protection industry co., LTD, Wuhan, China), a sampling and preconcentration

system for NMVOCs collection and enrichment, and a gas chromatography (GC, 7820A, Agilent Technologies, Santa Clara, CA, USA) equipped with an MS and an FID (5977E, Agilent Technology, Santa Clara, CA, USA) for NMVOCs separation and detection. The custom-built online GC-MS/FID was a two-channel system and was capable of measuring C2-C12 hydrocarbons and selected C2-C5 carbonyls. The two channels have their own inlets, cold traps and GC separation columns, but they share one cryogenic source and programmed temperature procedure. The availability of this system for NMVOCs measurement are well verified and it has been used in several large field campaign (Chen et al., 2014;Yuan et al., 2013;Wu et al., 2016), and was described by our previous paper (Yang et al., 2019). Briefly, samples are collected into GC-MS/FID at a flow rate of 60 mL min^{-1} with sampling time of 5 min at the beginning of each hour. The sampling lines for ambient air and standard gases were both Teflon tubes with a 1/4-inch outside diameter (OD). A Teflon filter was placed in the inlet to prevent particulate matters from entering the instrument, and a water trap was used to remove H_2O from the air samples. Ascarite II was used to remove CO_2 and O_3 before the FID channel, whereas a Na_2SO_3 trap was used to remove O_3 in the MS channel. C2-C5 hydrocarbons were separated on a PLOT-Al_2O_3 column (15 m × 0.32 mm ID×3 μm, J&W Scientific, USA) and were measured by the FID channel. Other compounds were separated on a semi polar column (DB624, 60 m × 0.25 mm ID×1.4 μm, J&W Scientific, USA) and were quantified using a quadrupole MS detector. The two columns were not exchanged during the intensive measurement campaign.

The compounds analyzed were subjected to rigorous quality assurance and quality control procedures (QA/QC). The NMVOCs detected by FID were quantified by the external standard method, and the components detected by MS were quantified by the internal standard method. Four compounds, i.e., bromochloromethane, 1,4-difluorobenzene, chlorobenzene-d5, and bromofluorobenzene, were used as internal standards. Specifically, the system was calibrated at multiple concentrations in the range of 0.8-8 ppb by two gas standards, i.e., a mixture of 57 PAMS (provided by Spectra Gases Inc., USA), and a mixture of oxygenated VOCs (OVOCs) and halocarbons (provided by Spectra Gases Inc., USA). R^2 values for the calibration curves ranged from 0.941 to 1.000 for NMVOCs, indicating that integral areas of the peaks were proportional to concentrations of target compounds. The method detection limit (MDL) of the online GC-FID/MS

system for all measured compounds ranged from 0.003 to 0.092 ppb. The measurement relative standard deviation (RSD) for measured compounds ranged from 2.1% to 14.9% (Yang et al., 2019). To check the stability of the instrument, routine calibration was performed periodically by using a calibration gas with a mixing ratio of 2 ppb consisting of 56 kinds of NMVOCs components. The variations between the measured and nominal concentrations of the periodic calibration were within 10%. The signal variations of each targeted compound due to system instability were corrected by the signal of CFC-113 (1,1,2-trichloro-1,2,2-trifluoroethane) due to its long atmospheric lifetime and stable anthropogenic emissions (Yuan et al., 2013;Chen et al., 2014). Detailed instrumental and operational parameters are described in our previous study (Yang et al., 2019).

Measurements of atmospheric HONO mixing ratios were conducted using a custom-made HONO analyzer. The detailed information can be seen elsewhere (Zhang et al., 2019;Tong et al., 2015). CH_4 were analyzed by Agilent 7890A gas chromatography (GC) with flame ionization detector (FID). Standard samples were provided by NIST of USA and NSC of China. The precision of CH_4 concentration analysis is 0.05± 0.10%. HCHO was measured by Hantzsch Fluorimetry with a commercial instrument (AL4021, Aerolaser GmbH, Germany) (Lu et al., 2019).

The photolysis frequencies, JO^1D, JNO_2 and JNO_3, in the atmosphere are measured by the PFS-100 Photolysis Spectrometer (Juguang Technology (hangzhou) Co., Ltd, Hangzhou, China). The photolysis rate is calculated by integrating the actinic flux with the known absorption cross section $\sigma(\lambda)$ and quantum yield $\varphi(\lambda)$. The actinic flux is spherically integrated photon radiance of the solar radiation in the atmosphere. The spectrometer obtains spectral information in a certain wavelength range, which mainly uses quartz receiver to collect solar radiation from all directions, and convert it into the actinic flux F_λ. $\sigma(\lambda)$ is the absorption cross section of the species that absorbs in certain wavelength range and $\varphi(\lambda)$ is quantum yield of the photodissociation reaction product; these two coefficients have been measured by experiments and can be directly looked up and used.

Figure captions

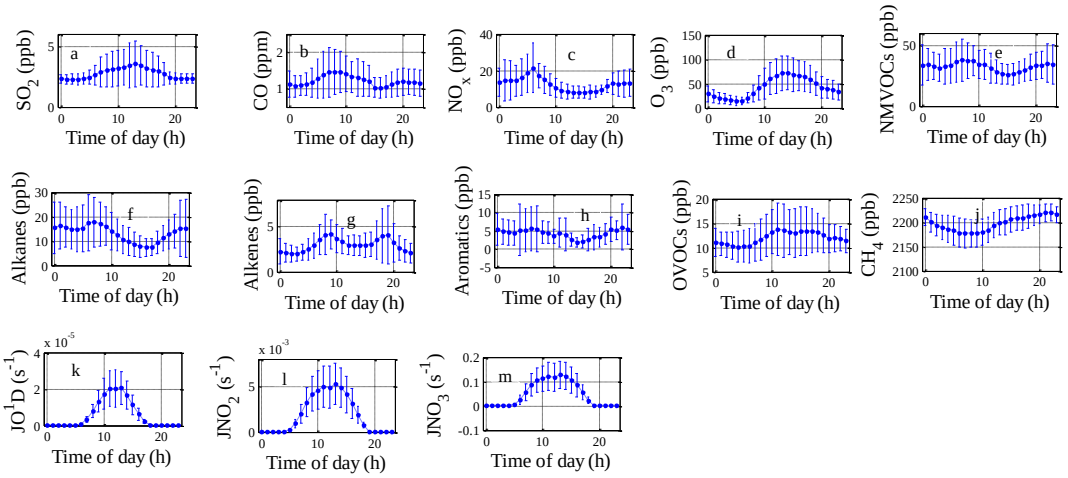

Figure S1. Mean diurnal variations of air pollutants and meteorological parameters observed during the field campaign at Xianghe from 6 July to 6 August 2018.

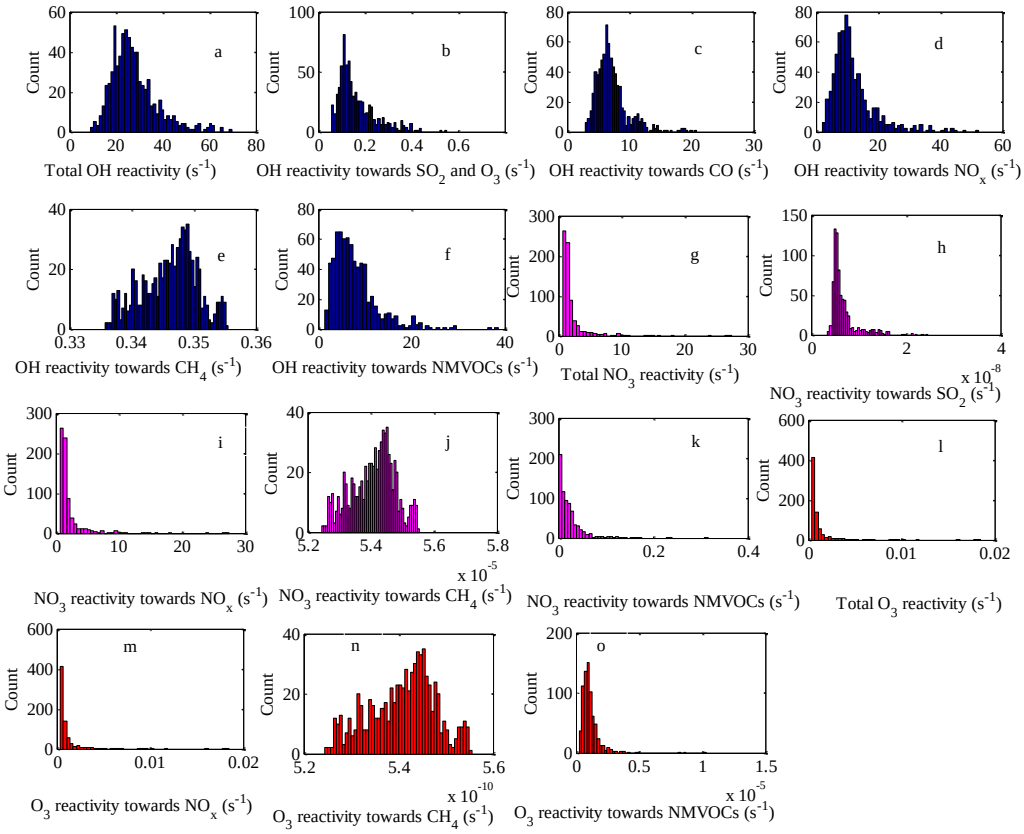

Figure S2. Frequency distributions of OH reactivity (a-f), NO_3 reactivity (g-k) and O_3 reactivity (l-o) of trace gases during the field campaign at Xianghe from 6 July to 6 August 2018.

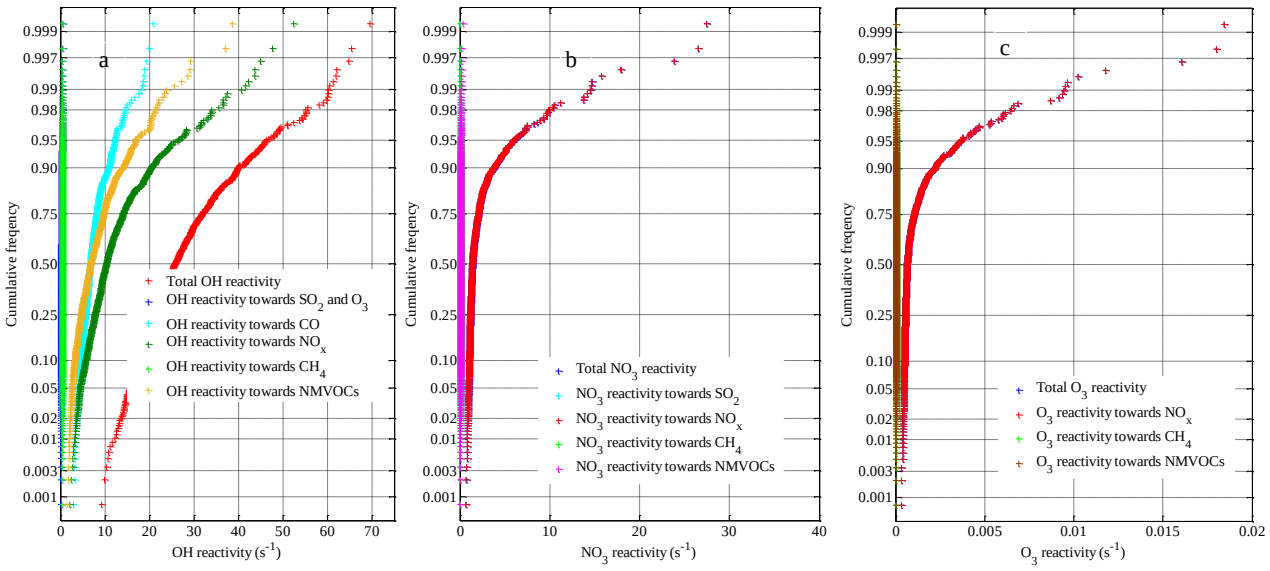

Figure S3. Cumulative frequency distributions of OH reactivity (a), NO_3 reactivity (b) and O_3 reactivity (c) of trace gases during the field campaign at Xianghe from 6 July to 6 August 2018.

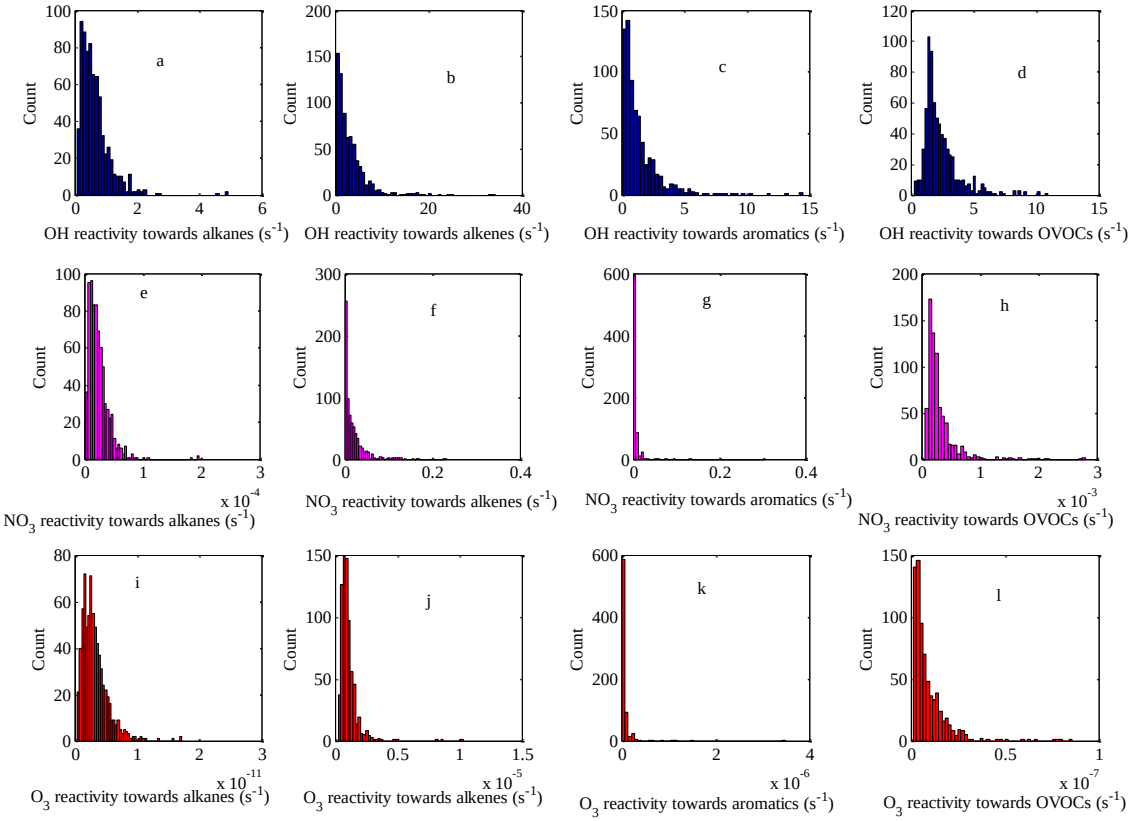

Figure S4. Frequency distributions of OH reactivity (a-d), NO_3 reactivity (e-h) and O_3 reactivity (i-l) of VOC groups during the field campaign at Xianghe from 6 July to 6 August 2018.

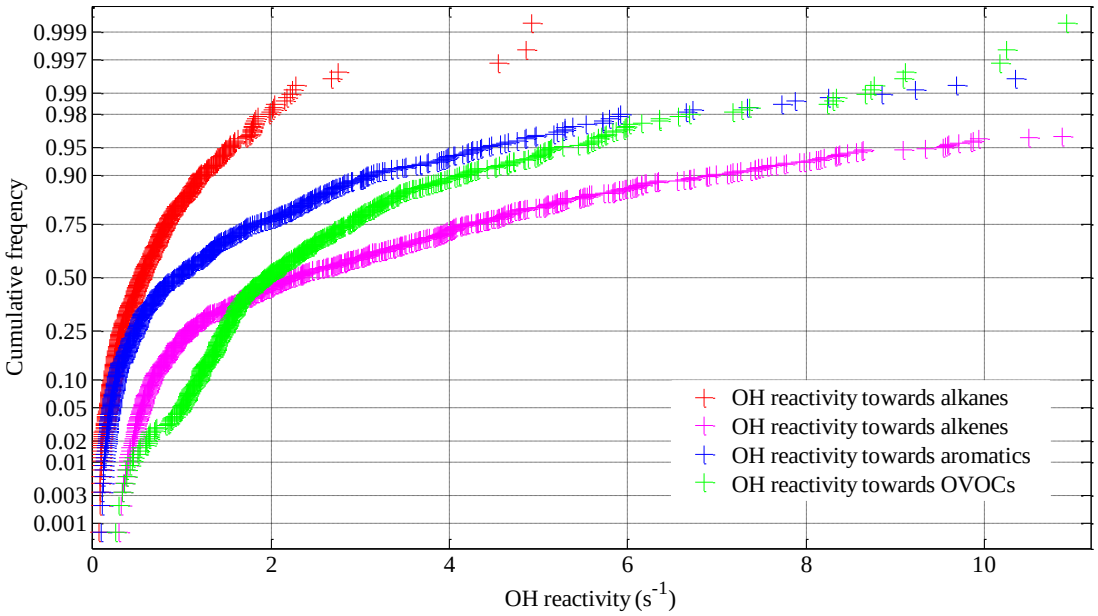

Figure S5. Cumulative frequency distributions of OH reactivity of NMVOCs groups during the field campaign at Xianghe from 6 July to 6 August 2018.

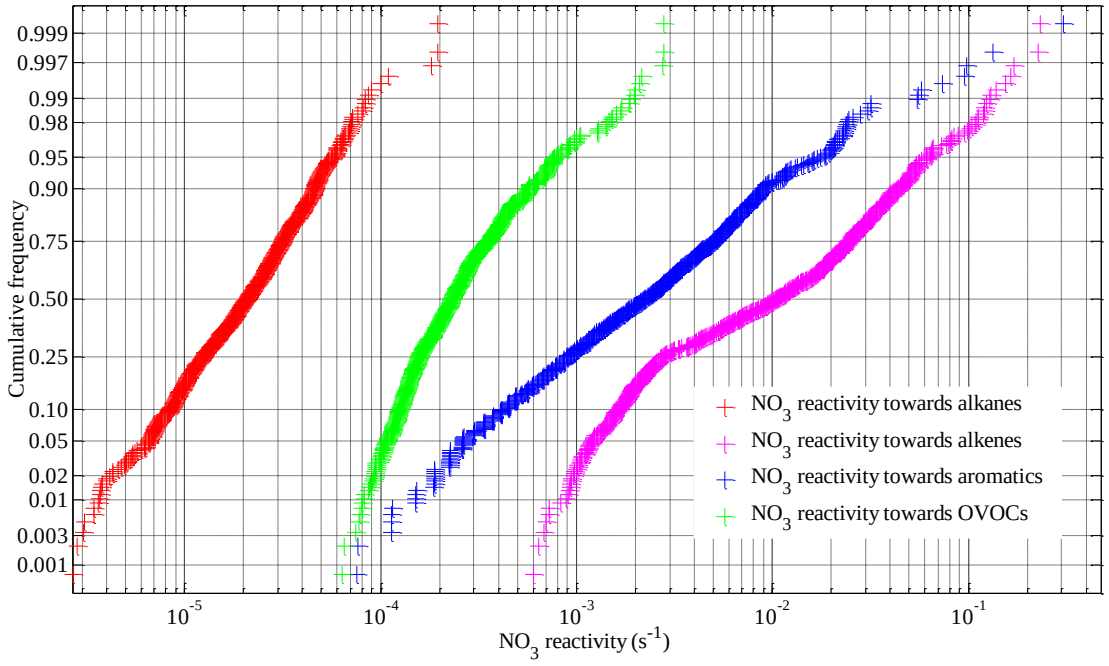

Figure S6. Cumulative frequency distributions of NO_3 reactivity of NMVOCs groups during the field campaign at Xianghe from 6 July to 6 August 2018.

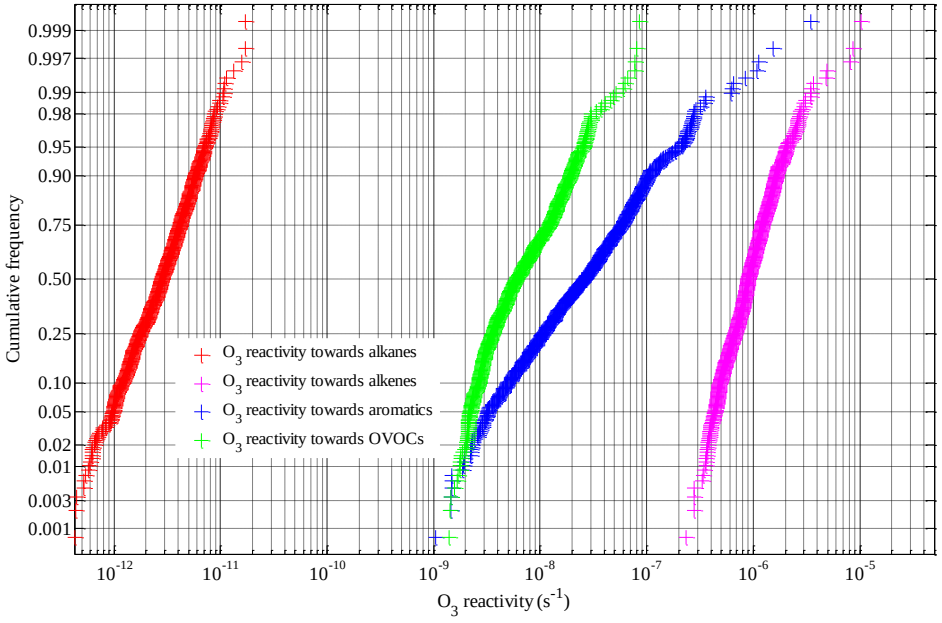

Figure S7. Cumulative frequency distributions of O_3 reactivity of NMVOCs groups during the field campaign at Xianghe from 6 July to 6 August 2018.

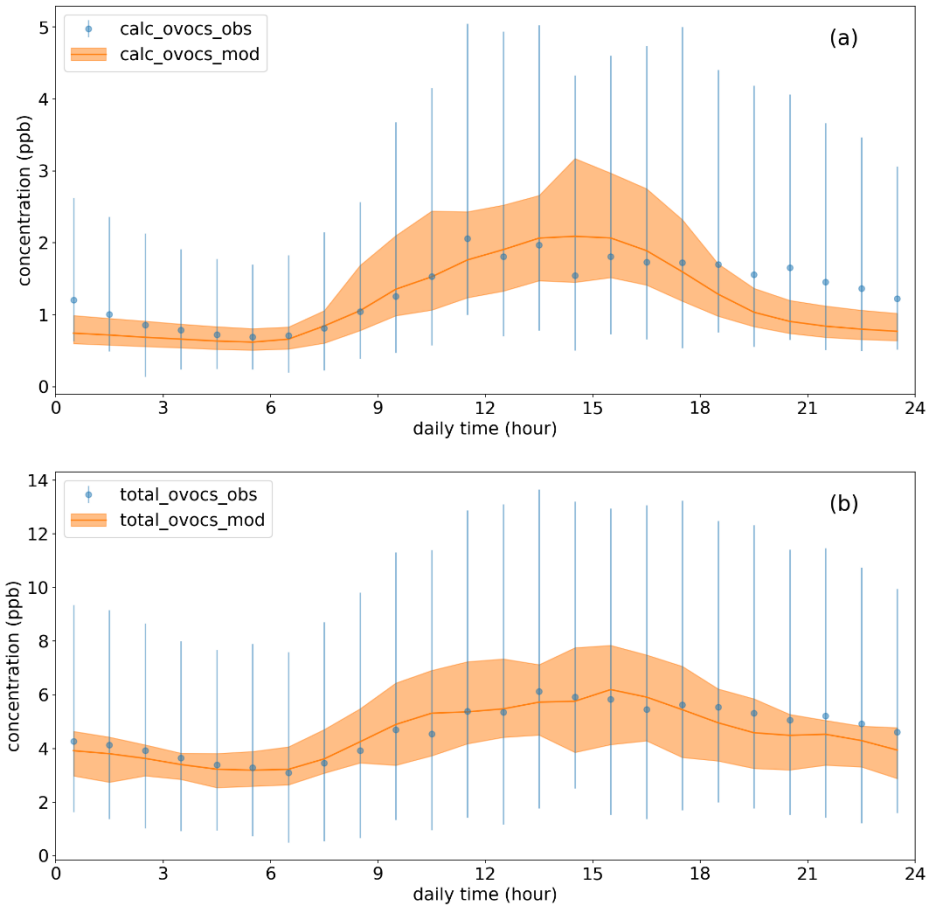

Figure S8: Diurnal mean of modeled (orange solid line) and measured (blue points) mixing ratios of (a) ten calculated and (b) all OVOCs, respectively. The ±1 standard deviation are also shown for modeled (orange shade) and measured (vertical sticks) data.

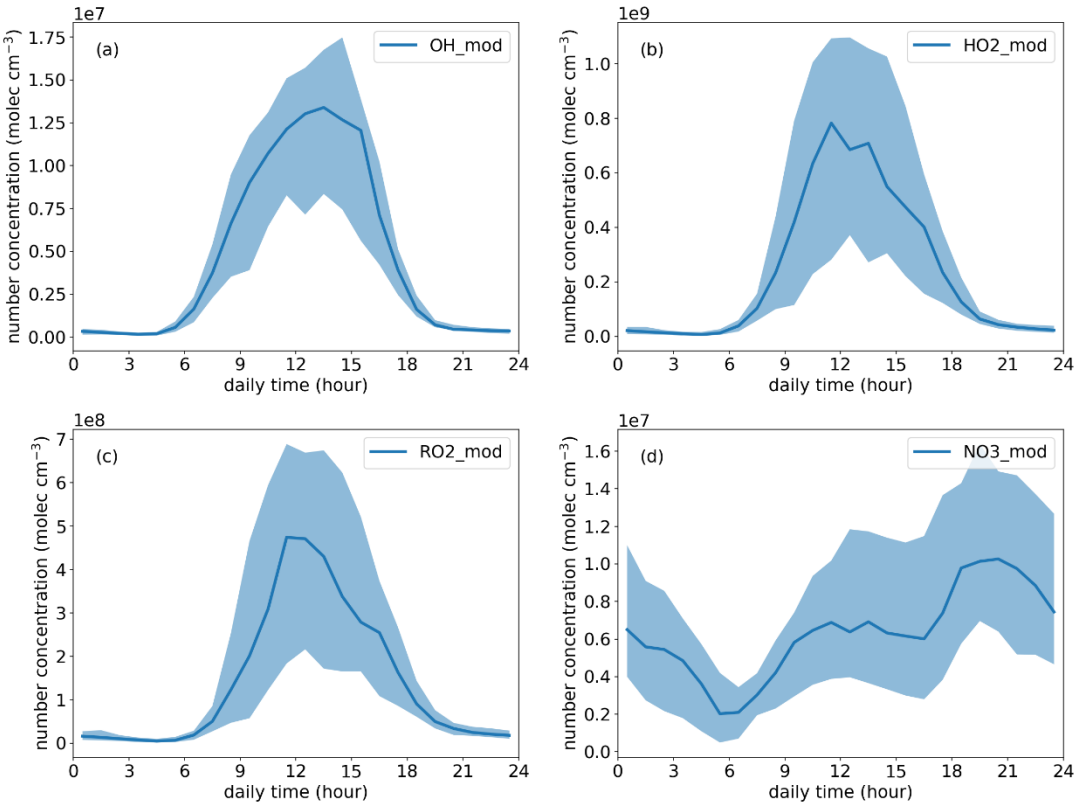

Figure S9: Modeled diurnal median (solid line) of (a) OH, (b) HO_2, (c) RO_2 and (d) NO_3. The 25th and 75th percentiles are shown as shade.

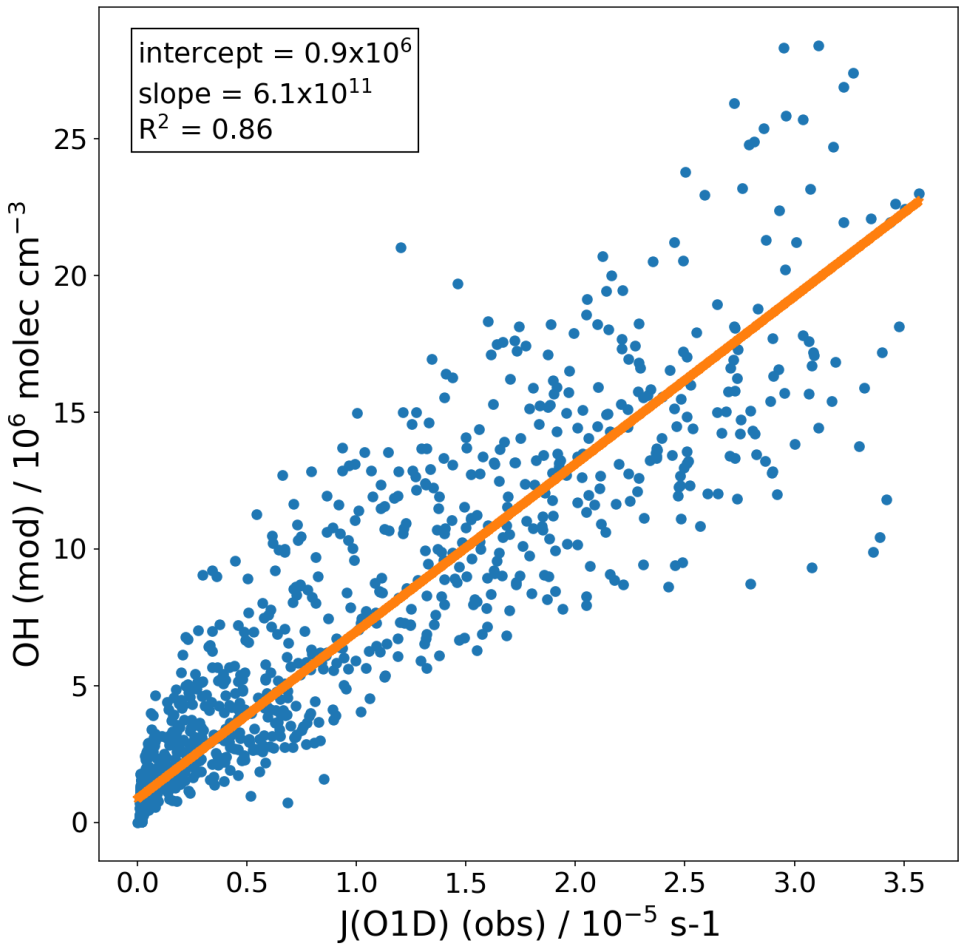

Figure S10: Correlation between modeled OH number concentration and measured JO^1D. A linear fit is shown by an orange line, the intercept, slope and R^2 values are shown in the legend.

Table captions

Table S1.The temperature-dependent reaction rate coefficients of trace gases with OH radical, O_3 and NO_3 radical used in this study.

Species	Temperature-dependence of k_{OH} (cm^3 $molecule^{-1}$ s^{-1})	Temperature-dependence of k_{O3} (cm^3 $molecule^{-1}$ s^{-1})	Temperature-dependence of k_{NO3} (cm^3 $molecule^{-1}$ s^{-1})
CH_4	$1.85\times10^{-12}\exp(-1690/T)$	$<1\times10^{-23}$	$<1\times10^{-18}$
	Alkanes		
Ethane	$6.9\times10^{-12}\exp(-1000/T)$	$<1\times10^{-23}$	$<1\times10^{-17}$
Propane	$7.6\times10^{-12}\exp(-585/T)\times0.736$	$<1\times10^{-23}$	$<7\times10^{-17}$
iso-Butane	$1.16\times10^{-17}\times T^2\times\exp(225/T)\times0.794$	$<1\times10^{-23}$	1.06×10^{-16}
n-Butane	$9.8\times10^{-12}\exp(-425/T)\times0.873$	$<1\times10^{-23}$	$2.8\times10^{-12}\exp(-3280/T)$
Cyclopentane	4.97×10^{-12}	$<1\times10^{-23}$	1.4×10^{-16}
iso-Pentane	3.6×10^{-12}	$<1\times10^{-23}$	1.62×10^{-16}
n-Pentane	$2.44\times10^{-17}\times T^2\times\exp(183/T)\times0.568$	$<1\times10^{-23}$	8.7×10^{-17}
2,2-Dimethylbutane	$3.22\times10^{-11}\exp(-781/T)\times0.632$	$<1\times10^{-23}$	4.4×10^{-16}
2,3-Dimethylbutane	$1.24\times10^{-17}\times T^2\times\exp(494/T)\times0.877$	$<1\times10^{-23}$	4.4×10^{-16}
2-Methylpentane	5.4×10^{-12}	$<1\times10^{-23}$	1.8×10^{-16}
3-Methylpentane	5.2×10^{-12}	$<1\times10^{-23}$	2.2×10^{-16}
n-Hexane	$1.53\times10^{-17}\times T^2\times\exp(414/T)\times0.061$	$<1\times10^{-23}$	1.1×10^{-16}
2,4-Dimethylpentane	4.77×10^{-12}	$<1\times10^{-23}$	1.5×10^{-16}
Methylcyclopentane	5.2×10^{-12}	$<1\times10^{-23}$	1.4×10^{-16}
2-Methylhexane	5.65×10^{-12}	$<1\times10^{-23}$	1.5×10^{-16}
2,3-Dimethylpentane	1.5×10^{-12}	$<1\times10^{-23}$	1.5×10^{-16}
Cyclohexane	$2.88\times10^{-17}\exp(309/T)$	$<1\times10^{-23}$	1.4×10^{-16}
3-Methylhexane	5.6×10^{-12}	$<1\times10^{-23}$	1.5×10^{-16}
2,2,4-Trimethylpentane	3.34×10^{-12}	$<1\times10^{-23}$	9.0×10^{-17}
n-Heptane	$1.59\times10^{-17}\times T^2\times\exp(478/T)$	$<1\times10^{-23}$	1.5×10^{-16}
Methylcyclohexane	4.97×10^{-12}	$<1\times10^{-23}$	1.4×10^{-16}
2,3,4-Trimethylpentane	6.6×10^{-12}	$<1\times10^{-23}$	1.9×10^{-16}

2-Methylheptane	7×10^{-12}	$<1\times10^{-23}$	1.9×10^{-16}
3-Methylheptane	7×10^{-12}	$<1\times10^{-23}$	1.9×10^{-16}
n-Octane	$2.76\times10^{-17}\times T^2\times\exp(378/T)$	$<1\times10^{-23}$	1.9×10^{-16}
Nonane	$2.51\times10^{-17}\times T^2\times\exp(477/T)$	$<1\times10^{-23}$	2.3×10^{-16}
n-Decane	$3.13\times10^{-17}\times T^2\times\exp(416/T)$	$<1\times10^{-23}$	2.8×10^{-16}
n-Undecane	12.3×10^{-12}	$<1\times10^{-23}$	
Alkenes			
Ethylene	$9.0\times10^{-12}\ (T/300)^{-0.85}$	$9.1\times10^{-15}\exp(-2580/T)$	$3.3\times10^{-12}\exp(-2880/T)$
Propylene	$3.0\times10^{-11}(T/300)^{-1}$	$5.5\times10^{-15}\exp(-1880/T)$	$4.6\times10^{-13}\exp(-1155/T)$
trans-2-Butene	$1.01\times10^{-11}\exp(550/T)$	$6.64\times10^{-15}\exp(-1095/T)$	3.9×10^{-13}
1-Butene	$6.6\times10^{-12}\exp(465/T)\times0.87$	9.64×10^{-18}	1.35×10^{-14}
cis-2-Butene	$1.1\times10^{-11}\exp(487/T)$	$3.22\times10^{-15}\exp(-968/T)$	3.52×10^{-13}
1,3-Butadiene	$1.48\times10^{-11}\exp(448/T)\times0.649$	$1.34\times10^{-14}\exp(-2283/T)\times0.5$	1.0×10^{-13}
1-Pentene	$5.86\times10^{-12}\exp(500/T)\times0.87$	1.06×10^{-17}	1.5×10^{-14}
trans-2-Pentene	6.7×10^{-11}	1.6×10^{-16}	3.7×10^{-13}
cis-2-Pentene	6.5×10^{-11}	1.3×10^{-16}	3.7×10^{-13}
Isoprene	$2.7\times10^{-11}\exp(390/T)$	$1.03\times10^{-14}\exp(-1995/T)$	$3.15\times10^{-12}\exp(-450/T)$
1-Hexene	3.7×10^{-11}	1.31×10^{-17}	1.8×10^{-14}
OVOCs			
HCHO	$5.4\times10^{-12}\exp(135/T)$	$<1\times10^{-20}$	5.6×10^{-16}
Acrolein	18.3	$<1\times10^{-20}$	
Propanal	$5.1\times10^{-12}\exp(405/T)$	$<1\times10^{-20}$	6.4×10^{-15}
Acetone	$8.8\times10^{-12}\exp(-1320/T)+$	$<1\times10^{-20}$	
	$1.7\times10^{-14}\exp(423/T)$		$<3\times10^{-17}$
MTBE	2.94×10^{-12}	$<1\times10^{-20}$	
Methacrolein	$8.0\times10^{-12}\exp(380/T)$	$1.4\times10^{-15}\exp(-2100/T)$	3.4×10^{-15}
n-Butanal	$6.0\times10^{-12}\exp(410/T)$	$<1\times10^{-20}$	$1.7\times10^{-12}\exp(-1500/T)$
MethylVinylKetone	$2.6\times10^{-12}\exp(610/T)$	$<1\times10^{-20}$	6.0×10^{-16}
Methylethylketone	$1.5\times10^{-12}\exp(-90/T)\times0.462$	$<1\times10^{-20}$	

2-Pentanone	4.4×10^{-12}	$<1\times10^{-20}$	
Pentanal	$6.34\times10^{-12}\exp(448/T)\times0.19$	$<1\times10^{-20}$	1.5×10^{-14}
3-Pentanone	2×10^{-12}	$<1\times10^{-20}$	
Hexanal	3.0×10^{-11}	$<1\times10^{-20}$	1.6×10^{-14}
Aromatics			
Benzene	$2.3\times10^{-12}\exp(-190/T)\times0.53$	$<1\times10^{-20}$	3.0×10^{-17}
Toluene	$1.8\times10^{-12}\exp(340/T)\times0.18$	$<1\times10^{-20}$	7.0×10^{-17}
Ethylbenzene	7×10^{-12}	$<1\times10^{-20}$	6.0×10^{-16}
m/p-Xylene	1.89×10^{-11}	$<1\times10^{-20}$	2.6×10^{-16}
o-Xylene	1.36×10^{-11}	$<1\times10^{-20}$	4.1×10^{-16}
Styrene	5.8×10^{-11}	1.7×10^{-17}	1.5×10^{-12}
Isopropylbenzene	6.3×10^{-12}	$<1\times10^{-20}$	6.0×10^{-16}
n-Propylbenzene	5.8×10^{-12}	$<1\times10^{-20}$	6.0×10^{-16}
m-Ethyltoluene	1.18×10^{-11}	$<1\times10^{-20}$	8.6×10^{-16}
p-Ethyltoluene	1.86×10^{-11}	$<1\times10^{-20}$	8.6×10^{-16}
1,3,5-Trimethylbenzene	5.67×10^{-11}	$<1\times10^{-20}$	8.8×10^{-16}
o-Ethyltoluene	1.19×10^{-11}	$<1\times10^{-20}$	8.6×10^{-16}
1,2,4-Trimethylbenzene	3.25×10^{-11}	$<1\times10^{-20}$	1.8×10^{-15}
1,2,3-Trimethylbenzene	3.27×10^{-11}	$<1\times10^{-20}$	1.9×10^{-15}
Criteria pollutants			
CO	2.4×10^{-13}		
NO	$3.3\times10^{-11}(T/300)^{-0.3}$	$1.4\times10^{-12}\exp(-1310/T)$	$1.8\times10^{-11}\exp(110/T)$
NO_2	4.1×10^{-11}	$1.4\times10^{-13}\exp(-2470/T)$	$1.9\times10^{-12}(T/300)^{0.2}$
SO_2	$1.3\times10^{-12}(T/300)^{-0.7}$		$<1.0\times10^{-19}$
O_3	$1.7\times10^{-12}\exp(-940/T)$		

The temperature-dependent reaction rate coefficients are from (Atkinson et al., 1983), (Atkinson and Arey, 2003), (Atkinson et al., 2006), (Salgado et al., 2008) and the Master Chemical Mechanism, MCM v3.3.1 via the website: http://mcm.leeds.ac.uk/MCM (last accessed: 25 March 2020); *The temperature-dependent reaction rate coefficients* of NO, NO_2, SO_2 and O_3 are from (Atkinson et al., 2004). T denotes temperature.

References

Atkinson, R., Aschmann, S. M., and Jr., J. N. P.: Kinetics of the gas-phase reactions of OH radicals with a series of α,β-unsaturated carbonyls at 299 ± 2 K, International Journal of Chemical Kinetics, 15, 75-81, doi:10.1002/kin.550150108, 1983.

Atkinson, R., and Arey, J.: Atmospheric Degradation of Volatile Organic Compounds., Chemical Reviews, 103, 4605-4638, doi:10.102/cr0206420, 2003.

Atkinson, R., Baulch, D. L., Cox, R. A., Crowley, J. N., Hampson, R. F., Hynes, R. G., Jenkin, M. E., Rossi, M. J., and Troe, J.: Evaluated kinetic and photochemical data for atmospheric chemistry: Volume I - gas phase reactions of Ox, HOx, NOx and SOx species, Atmos. Chem. Phys., 4, 1461-1738, doi:10.5194/acp-4-1461-2004, 2004.

Atkinson, R., Baulch, D. L., Cox, R. A., Crowley, J. N., Hampson, R. F., Hynes, R. G., Jenkin, M. E., Rossi, M. J., Troe, J., and IUPAC Subcommittee: Evaluated kinetic and photochemical data for atmospheric chemistry : Volume II - gas phase reactions of organic species, Atmos. Chem. Phys., 6, 3625-4055, doi:10.5194/acp-6-3625-2006, 2006.

Chen, W. T., Shao, M., Lu, S. H., Wang, M., Zeng, L. M., Yuan, B., and Liu, Y.: Understanding primary and secondary sources of ambient carbonyl compounds in Beijing using the PMF model, Atmos Chem Phys, 14, 3047-3062, doi:10.5194/acp-14-3047-2014, 2014.

Lu, K., Fuchs, H., Hofzumahaus, A., Tan, Z., Wang, H., Zhang, L., Schmitt, S. H., Rohrer, F., Bohn, B., Broch, S., Dong, H., Gkatzelis, G. I., Hohaus, T., Holland, F., Li, X., Liu, Y., Liu, Y., Ma, X., Novelli, A., Schlag, P., Shao, M., Wu, Y., Wu, Z., Zeng, L., Hu, M., Kiendler-Scharr, A., Wahner, A., and Zhang, Y.: Fast Photochemistry in Wintertime Haze: Consequences for Pollution Mitigation Strategies, Environ Sci Technol, 53, 10676-10684, doi:10.1021/acs.est.9b02422, 2019.

Salgado, M. S., Monedero, E., Villanueva, F., Martín, P., Tapia, A., and Caba?as, B.: Night-Time Atmospheric Fate of Acrolein and Crotonaldehyde, Environ Sci Technol, 42, 2394-2400, doi:10.1021/es702533u, 2008.

Tong, S., Hou, S., Zhang, Y., Chu, B., Liu, Y., He, H., Zhao, P., and Ge, M.-F.: Exploring the nitrous acid (HONO) formation mechanism in winter Beijing: direct emissions and heterogeneous production in urban and suburban areas, Faraday Discuss., 189, doi:10.1039/C5FD00163C, 2015.

Wang, Y. H., Hu, B., Ji, D. S., Liu, Z. R., Tang, G. Q., Xin, J. Y., Zhang, H. X., Song, T., Wang, L.

L., Gao, W. K., Wang, X. K., and Wang, Y. S.: Ozone weekend effects in the Beijing–Tianjin–Hebei metropolitan area, China, Atmos Chem Phys, 14, 2419-2429, doi:10.5194/acp-14-2419-2014, 2014.

Wu, R., Li, J., Hao, Y., Li, Y., Zeng, L., and Xie, S.: Evolution process and sources of ambient volatile organic compounds during a severe haze event in Beijing, China, Sci Total Environ, 560-561, 62-72, doi:10.1016/j.scitotenv.2016.04.030, 2016.

Xin, J. Y., Wang, Y. S., Tang, G. Q., Wang, L. L., Sun, Y., Wang, Y. H., Hu, B., Song, T., Ji, D. S., and Wang, W. F.: Variability and reduction of atmospheric pollutants in Beijing and its surrounding area during the Beijing 2008 Olympic Games, Chinese Sci Bull, 55, 1937-1944, doi: 10.1007/s00376-012-1227-4, 2012.

Yang, Y., Ji, D., Sun, J., Wang, Y., Yao, D., Zhao, S., Yu, X., Zeng, L., Zhang, R., Zhang, H., Wang, Y., and Wang, Y.: Ambient volatile organic compounds in a suburban site between Beijing and Tianjin: Concentration levels, source apportionment and health risk assessment, Sci Total Environ, 695, 133889, doi:10.1016/j.scitotenv.2019.133889, 2019.

Yuan, B., Hu, W. W., Shao, M., Wang, M., Chen, W. T., Lu, S. H., Zeng, L. M., and Hu, M.: VOC emissions, evolutions and contributions to SOA formation at a receptor site in eastern China, Atmos Chem Phys, 13, 8815-8832, doi:10.5194/acp-13-8815-2013, 2013.

Zhang, W., Tong, S., Ge, M.-F., An, J., Shi, Z., Hou, S., Xia, K., qu, y., Zhang, H., Chu, B., Sun, Y., and He, H.: Variations and sources of nitrous acid (HONO) during a severe pollution episode in Beijing in winter 2016, Sci Total Environ, 648, doi:10.1016/j.scitotenv.2018.08.133, 2019.